Template Synthesis of NPN' Pincer-type Ligands at Titanium Using an Ambiphilic Phosphide Scaffold

Alex Moerman, E. Daiann Sosa Carrizo, Benjamin Théron, Hélène Cattey, Pierre Le Gendre, Paul Fleurat-Lessard, Adrien Normand

Template Synthesis of NPN' Pincer-Type Ligands at Titanium Using an Ambiphilic Phosphide Scaffold

Alex Moerman, E. Daiann Sosa Carrizo, Benjamin Théron, Hélène Cattey, Pierre Le Gendre, Paul Fleurat-Lessard and Adrien T. Normand**

Institut de Chimie Moléculaire de L'Université de Bourgogne (ICMUB), Université de Bourgogne, 9 avenue Alain Savary, 21000 Dijon (FR)

Abstract

Ti-imido complex [TiCl(N^{t}Bu)(BIPP)] (**1**; BIPP = bis(iminophosphoranyl)phosphide ligand) reacts with terminal alkynes R–C≡CH (R = phenyl, isopropenyl, cyclopropyl, 2-pyridyl) via P-P bond cleavage of the BIPP ligand. The resulting complexes [TiCl(NPN')(NPhPPh$_2$)] (**2a-d**) contain a pincer-type NPN' phosphide ligand that incorporates the terminal alkyne and the imido ligand from complex **1**. Complexes **2a-d** feature two chiral centers (Ti and P) with interdependent absolute configurations, thus they are formed stereoselectively. Complex **2a** (R = phenyl) undergoes chloride abstraction with [Et$_3$SiHSiEt$_3$][B(C$_6$F$_5$)$_4$], yielding [Ti(NPN')(NPhPPh$_2$)][B(C$_6$F$_5$)$_4$] (**3**). Complex **3** is a moderately active and stereoselective initiator for the ring-opening polymerization of *rac*-lactide. Complex **3** activates the C=O bond of 4-iodobenzaldehyde to give complex **4** as a single diastereomer despite the presence of three chiral centers. Complex **3** undergoes transmetallation with SbCl$_3$, yielding [Sb(NPN')][B(C$_6$F$_5$)$_4$] (**5**) and

[$TiCl_3(NPhPPh_2)$] (**6**) selectively. The bonding situation in **3** and **5** was analyzed using Bader's Atoms-In-Molecules (AIM) and the Electron Localization Function (ELF), showing that the nitrogen atoms of the NPN' ligand are electronically similar, and that the metal-phosphide interaction is more polar in the case of titanium.

Introduction

Dicoordinate phosphorus compounds span a wide spectrum of reactivities, from Lewis basic phosphides (**I**) to phosphinyl radicals (**II**) and Lewis acidic phospheniums (**III**) (Chart 1).[1-4] For instance, compounds **A**, **B** and **C** belong to these categories, and thus react accordingly (Chart 2).[5-10] However, although the difference between phosphides and phospheniums seems obvious, the electronic properties of substituents X can somewhat blur the distinction between these two classes of compounds.[11] Thus, phosphide **D** and phosphenium **E** (which respectively contain electron-withdrawing and electron-donating substituents) both display ambiphilic character.[12-16] In extreme cases, net charges become all but insignificant: compound **F** can bind up to two metal centres,[17-19] which clearly makes it a competent Lewis base.[20]

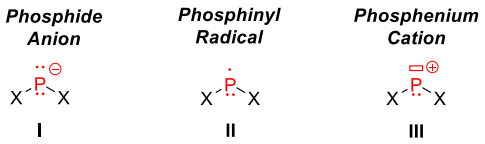

Chart 1. Main Types of dicoordinate phosphorus compounds.

The reactivity of **F** can be explained by the fact that the ylidic groups impart considerable electron density to the central phosphorus atom,[21] to the extent that this cationic compound may actually be described as a bisphosphonio-substituted isophosphindolide (resonance form **F**-).[20] Other strongly-donating substituents, such as N-heterocyclic olefins, may achieve similar results.[22]

Conversely, strongly electron-withdrawing substituents, such as the cyano group (**D**), can confer electrophilic character to phosphides.[12-14]

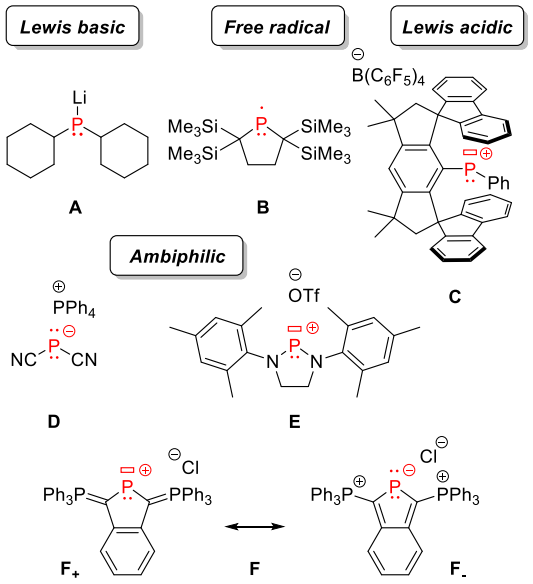

Chart 2. Literature examples of dicoordinate phosphorus compounds.

We have recently reported the use of bis(iminophosphoranyl)phosphide anions (BIPP) as ligands for transition metals.[23] BIPP are valence isoelectronic to bis(iminophosphoranyl)methanediides (BIPM), which can be considered as P(V)-stabilized geminal dianions.[24, 25] However, BIPP can hardly be described as classical phosphide ligands: for instance in complex **1** (Chart 3), the electron-withdrawing effect of the substituents is such that the negatively charged central phosphorus atom only interacts electrostatically with Ti. In fact, the low-lying (-1.61 eV) LUMO of **1** displays P-P antibonding character, which suggests that the central phosphorus atom could be sensitive to nucleophilic attack.[23]

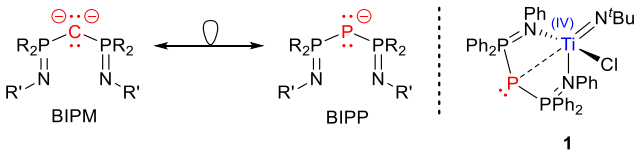

Chart 3. Left: isolobal relationship between BIPM and BIPP ligands. Right: a previously reported Ti-BIPP complex.[26]

Overall, experimental and computational evidence indicates that BIPP complexes are closely related to ambiphilic triphosphenium cations (TP), another type of dicoordinate phosphorus compounds.[27-29] This analogy can be understood by considering the depiction of BIPP and TP using the arrow formalism (Chart 4).[30] The well-documented — and synthetically useful — propensity of TP to undergo P-P bond cleavage thus suggests that BIPP and their complexes could be amenable to similar transformations.[31-40]

Chart 4. A BIPP ligand depicted as a TP with amidophosphine substituents.

In this contribution, we report the serendipitous discovery of P-P bond cleavage in complex **1** by Ti-activated terminal alkynes. This reactivity enables the template synthesis of elaborate NPN' pincer-type ligands at Titanium. We further demonstrate the practicability of this methodology by transferring one of the NPN' ligands to antimony.

Results and discussion

Experimental results

Titanium imido complexes are useful precatalysts in hydroamination catalysis,[41-45] therefore we initially tested the behavior of **1** in the presence of aniline and phenylacetylene (5 % [Ti], C_6D_6,

105 °C, 24 h). However, the results were disappointing: very little conversion to the hydroamination products was observed (see Figure S66). In order to uncover the reasons behind this poor catalytic activity, we investigated the behavior of **1** towards phenylacetylene alone: indeed, imido complexes of group 4 metals typically undergo [2+2] cycloaddition with alkynes.[44, 46] We monitored a CD_2Cl_2 solution of **1** (0.1 mmol) with 1 eq of phenylacetylene by NMR spectroscopy (4 days, room temperature). The $^{31}P\{^1H\}$ NMR spectrum of the reaction mixture revealed almost complete conversion to a new compound, featuring three distinct signals in a 1:1:1 ratio (Figure 1). Moreover, the diagnostic triplet at -179.2 ppm corresponding to the central phosphorus was replaced by a doublet at -62.3 ppm ($^1J_{PP}$ = 350 Hz). These observations suggested a much more drastic evolution than just a simple desymmetrization of the BIPP ligand's environment (*e.g.* caused by a change in the coordination sphere of Ti consecutive to alkyne insertion).

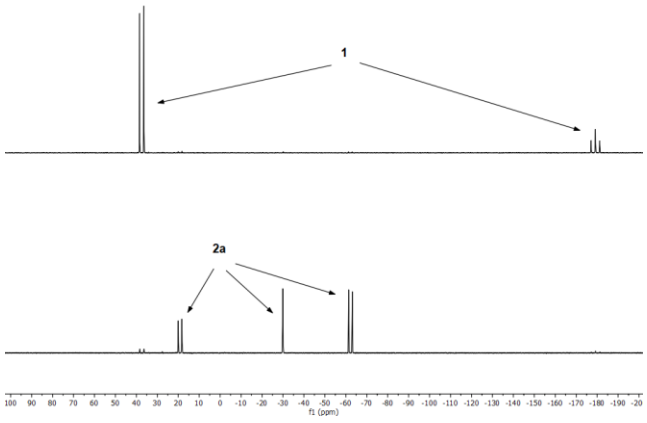

Figure 1. $^{31}P\{^1H\}$ NMR spectra of the reaction of complex **1** with phenylacetylene in CD_2Cl_2 (top: t0; bottom: t0 + 4 days).

We repeated the reaction on preparative scale and complex **2a** was isolated as a dark brown powder in 79 % yield (Scheme 1). Other terminal alkynes led to similar outcomes (**2b-d**), however

no reaction was observed with 1-phenyl-1-propyne. Likewise, isoprene (a 1,3-diene) also failed to react.

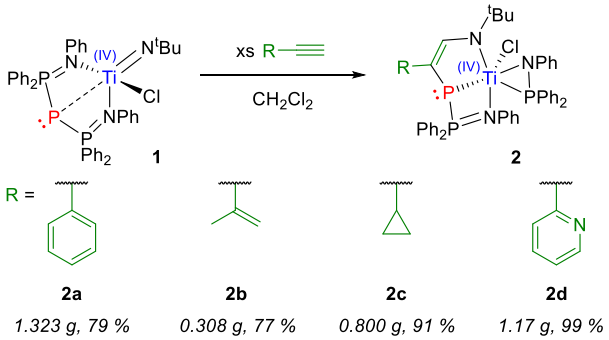

Scheme 1. Synthesis of complexes **2a-d**.

The ^{1}H, ^{13}C{^{1}H} and ^{31}P{^{1}H} NMR spectra of complexes **2a-d** display several characteristic features (Table 1). The olefinic proton (H2) resonates as a strongly deshielded doublet of doublet (because of scalar coupling with the phosphorus atoms of the P-P moiety), around 7.5-8.6 ppm. The chemical shift of H2 appears to be quite sensitive to the electronic nature of R: thus, it is the most shielded in **2c** (R = cyclopropyl), and the most deshielded in **2d** (R = 2-pyridyl). The corresponding C2 carbon also resonates as a strongly deshielded doublet of doublet, around 152-160 ppm, and its chemical shift follows the same trend as H2. By contrast, the quaternary olefinic C1 carbon is strongly shielded (109-116 ppm) and follows an inverse trend, *i.e.* it is most shielded in **2d**, and most deshielded in **2c**.

No clear trends can be established for the ^{31}P{^{1}H} NMR parameters. The three moieties (phosphide: P1; phosphoranyl: P2; phosphine: P3) give rise to well separated signals (P1: -62 to -67 ppm; P2: 17 to 20 ppm; P3: -22 to -30 ppm). A large ^{1}J scalar coupling can be observed between P1 and P2 for **2a-d** ($^{1}J_{P1P2}$ = 330-360 Hz), although it is smaller than in complex **1** (416 Hz).[24] Additional small ^{2}J and ^{3}J coupling through Ti can be measured for **2a-c** ($^{2}J_{P1P3}$, $^{3}J_{P2P3} \approx 7$ Hz).

Single crystals of **2a-d** suitable for X-ray diffraction analysis were obtained by vapor diffusion of pentane into solutions of those complexes in CH_2Cl_2 at -18 °C (Figure 2). Relevant bond distances and angles are gathered in Table 2.[47]

Table 1. Selected NMR parameters for **2a-d** and **3**-**5**.[a]

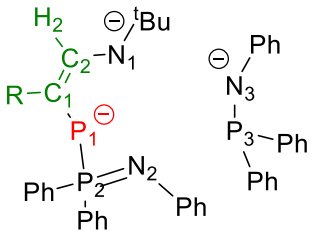

	2a	**2b**	**2c**	**2d**	**3**	**4**	**5**
δ_{C1}	111.0	114.7	116.2	109.5	115.4	110.4	99.6
δ_{C2}	153.0	157.5	152.4	159.5	143.9	151.8	155.2
δ_{H2}	7.97	7.60	7.52-7.46	8.60	8.59	7.89	8.41
δ_{P1}	-62.3	-67.2	-63.0	-64.4	-8.8	-76.2	-52.5
δ_{P2}	19.1	20.1	18.0	17	3.4	-6.6	100.1
δ_{P3}	-29.9	-22.6	-27.2	-27.1	-0.2	70.5	N.A.
$^1J_{P1P2}$	350	336	357	347	369	383	306
$^2J_{P1P3}$	6.8	7.2	7.3	N.A.	N.A.	N.A.	N.A.
$^3J_{P2P3}$	7.0	7.3	6.5	N.A.	N.A.	N.A.	N.A.

[a]: δ values in ppm, *J* values in Hz.

Complexes **2a-d** are chiral at titanium, due to a highly differentiated coordination environment: indeed, all the atoms bound to Ti are chemically non-equivalent. Moreover, the NPN' ligand is P-stereogenic due to the pyramidalization of P1.[48] Therefore, in theory, these compounds can exist as several diastereomers. Obviously, the exact number of possible diastereomers depends on the geometry of the complexes, which is not trivial in the case of **2a-d** (*vide infra*). However, the configuration of P1 appears to be determined by the coordination environment of the metal: indeed,

the orientation of the C1-C2 bridge depends on the position of N1 (*i.e.* away from the bulky amidophosphine ligand). Thus, in practice, complexes **2a-d** crystallize as a single diastereomer, consistent with the observed behavior in solution.[49] For complex **2d**, the crystal cell actually contains two independent molecules of the same diastereomer (**2d-1** and **2d-2**).[50]

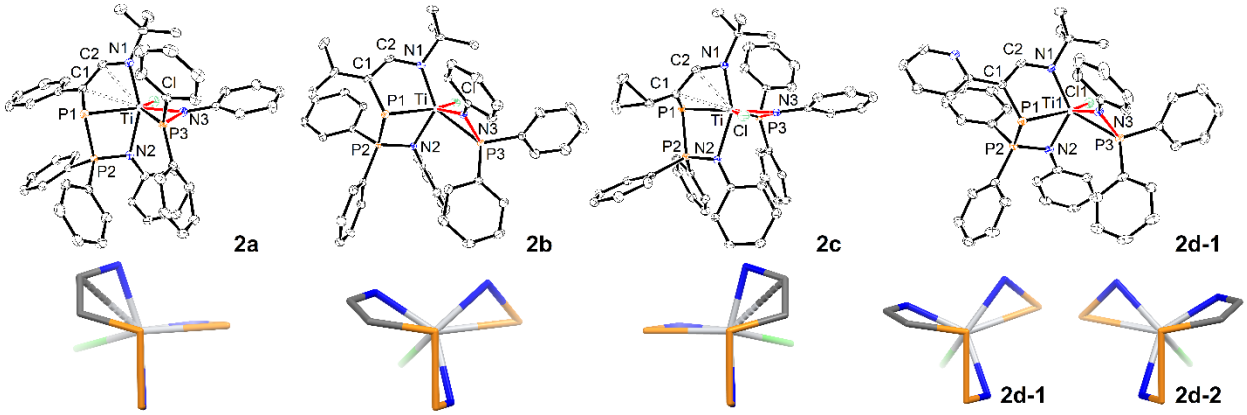

Figure 2. Top: ORTEP depiction of the X-ray structures of **2a-d**; asymmetric unit only; thermal ellipsoids drawn at the 50% probability level; solvent molecules and hydrogen atoms are not shown for clarity; for **2d** only one of the independent molecules present in the asymmetric unit is shown **(2d-1**); P3-N3-Ti-Cl torsion angle highlighted in red (P3-N3-Ti1-Cl1 for **2d-1**); see Table 2 for metric parameters. Bottom: Capped sticks depiction of the first coordination sphere of the metal in **2a-d**, viewed along the Ti-P1 bond (Ti1-P1 for **2d-1**).

As mentioned above, the geometry of **2a-d** is complex, due to the combination of geometrical constraints and a hexacoordinate environment. For simplicity, the two coordination sites occupied by the amidophosphine ligand (P3N3) can be considered as one. With this hypothesis, **2a** and **2c** can be described as distorted trigonal bipyramids in which the NPN' ligand binds Ti in *mer*-like fashion. Note that in this case, the amidophosphine ligand is oriented parallel to the Ti-Cl bond (P3-N3-Ti-Cl torsion angle close to ± 170 °). The first coordination sphere of Ti is completed by

C1 and C2, which "fold back" towards the metal, although the distances between these atoms and Ti (2.427(3) to 2.661(2) Å) are probably too high for a covalent interaction (the sum of covalent radii for Ti and C_{sp2} is 2.43±0.10 Å).[51]

Table 2. Selected bond distances (Å) and angles (°) for complexes **2a-d** and **3**

		2a	**2b**	**2c**	**2d-1**[a]
2a,c > 2b,d	C1-C2	1.375(3)	1.355(2)	1.378(4)	1.352(4)
	Ti-N2	2.1635(16)	2.0774(12)	2.194(2)	2.104(2)
	Ti-N3	2.0165(16)	1.9739(12)	2.023(2)	1.983(2)
	Ti-Cl	2.3864(6)	2.3555(4)	2.4072(8)	2.3440(8)
	P1-P2	2.1541(7)	2.1340(5)	2.1471(9)	2.1376(10)
	N1-Ti-N2	153.73(7)	128.25(5)	152.79(9)	125.99(9)
	P3-N3-Ti-Cl[b]	-168.12(5)	-53.05(6)	167.03(8)	-52.94(12)
2a,c < 2b,d	Ti-C1	2.661(2)	3.2716(15)	2.520(3)	3.308(3)
	Ti-C2	2.514(2)	2.9532(16)	2.427(3)	2.985(3)
	Ti-N1	1.9765(16)	1.9992(12)	1.971(2)	2.009(2)
	Ti-P1	2.5496(6)	2.5987(5)	2.5369(8)	2.5904(8)
	Ti-P3	2.4394(6)	2.5450(5)	2.4490(8)	2.5262(8)
	P3-N3	1.6520(16)	1.6690(12)	1.650(2)	1.663(2)
	Σα(P1)	251.58(10)	270.92(8)	246.07(12)	270.90(13)
No Trend	P2-N2	1.6297(16)	1.6261(12)	1.623(2)	1.630(2)
	C1-P1-P2[b]	101.90(7)	99.89(5)	99.59(9)	99.32(9)

[a]: for **2d-1**, Ti corresponds to Ti1 and Cl corresponds to Cl1. [b]: absolute values are considered for classification purposes.

Compounds **2b** and **2d** show even more distorted geometries due to a different orientation of the amidophosphine ligand (P3-N3-Ti-Cl torsion angle close to - 50 °, see Figure 2, bottom). As a result, the NPN' ligand deviates considerably from the *mer*-like coordination mode observed in **2a**

and **2c** (N1-Ti-N2 angle close to 127 ° instead of 153 °). As a matter of fact, most of the parameters listed in Table 2 follow the dichotomy between **2a,c** and **2b,d**: some bond distances (*e.g.* Ti-C1, Ti-C2, Ti-N1, Ti-P1 and Ti-P3) are considerably shorter in **2a,c** than in **2b,d**, while the reverse is true for some others (*e.g.* Ti-N2, Ti-N3 and Ti-Cl). An interesting consequence is the more relaxed conformation of the NPN' ligand in **2b,d** due to the absence of interactions between Ti and C1/C2. Thus, the most salient geometrical differences observed for **2a-d** appear to be (mostly) due to conformational changes.

Perhaps the most interesting feature of complexes **2a-d** is the short mean Ti-P1 distance (2.57 Å), just within the sum of covalent radii for Ti and P (2.67±0.11 Å).[51] This suggests a (polarized) covalent bond between these atoms (*vide infra*), in contrast with the weak electrostatic interaction between Ti and the central phosphorus atom of the BIPP ligand in complex **1** (d_{Ti-P1} = 3.0308(7) Å). Yet, the sum of angles around P1 is unusually low for a metal phosphide: around 250 ° in **2a-c**, 270 ° in **2b-d**. Metal phosphides generally display trigonal pyramidal or trigonal planar geometries, depending on the presence of d electrons on the metal.[52] Indeed, we have previously observed an almost perfect trigonal planar geometry in Ti(IV)-phosphides.[53] In the case of **2a-d**, the extreme pyramidalization of P1 is likely a result of the geometrical constraints imposed by the NPN' ligand framework.

In summary, the reaction of **1** with terminal alkynes transforms a BIPP ligand into a pincer-type phosphide ligand. The expansion of the BIPP ring and the replacement of one of its iminophosphoranyl side-arms by a more basic substituent both contribute to strengthen the Ti-P interaction, as revealed by the dramatic shortening of the Ti-P1 bond. Two mechanisms (**A** and **B**) can be envisaged for this reaction (Scheme 2).[54] The cleavage of the P-P bond could occur first, yielding a phosphinidene intermediate (**A1**), which would then undergo [2+1] cycloaddition with the terminal alkyne, yielding a Ti-bound phosphirene (**A2**). This mechanism is reminiscent of the

reactivity of masked phosphinidenes reported by Marinetti and Mathey.[55] Additionally, phosphirene **A2** would be expected to undergo nucleophilic ring-opening.[56] However, if a phosphinidene intermediate (*i.e.* **A1** minus the alkyne) was indeed generated, it would undoubtedly react with isoprene or 1-phenyl-1-propyne to generate a phosphirene.[55] Thus, the absence of reaction with these substrates mitigates against mechanism A.

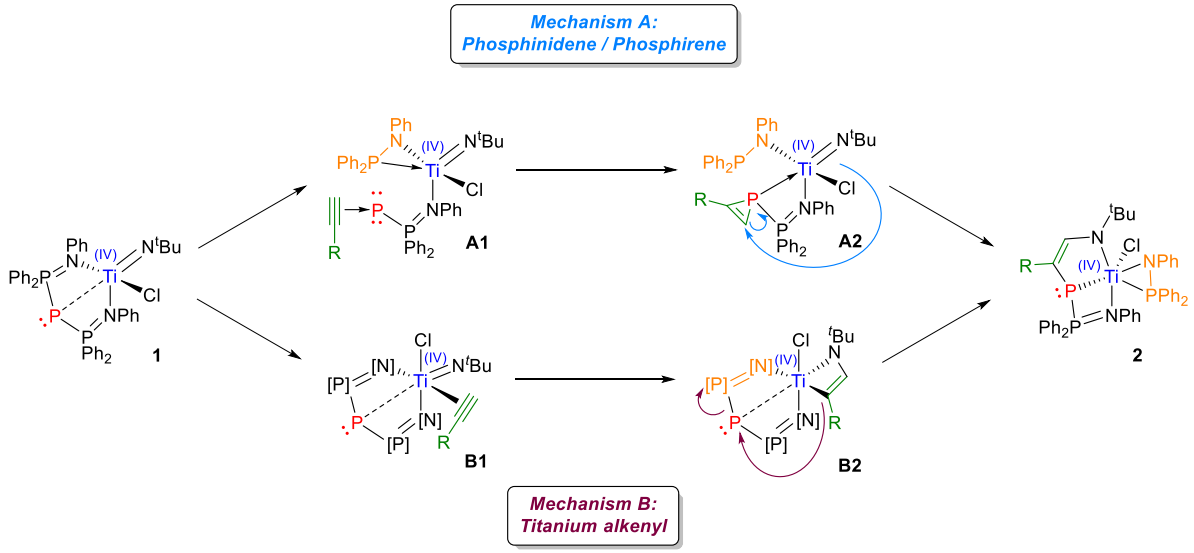

Scheme 2. Possible mechanisms for the formation of **2**.

The most probable mechanism — based on both experimental evidence and chemical intuition — involves initial activation of the alkyne by [2+2] cycloaddition with the Ti-imido moiety from intermediate **B1**.[44, 46] The central phosphorus atom of the BIPP ligand would then undergo nucleophilic substitution by the Ti-bound alkenyl ligand in **B2**, yielding **2**. Indeed, the results of DFT calculations (see the computational details) are consistent with this mechanism, for which the largest computed free energy barrier is 23.7 kcal.mol^{-1} (for **B2→2a'**, Figure 3).[57] By contrast, the largest computed barrier for mechanism **A** is 43.1 kcal.mol^{-1} (Figure S74). Interestingly, P-P bond cleavage does not yield **2a** directly, but rather its diastereomer (**2a'**), which is the kinetic product

of the reaction. However, the isomerization barrier is quite low (12.9 kcal.mol^{-1}), and the experimentally observed diastereomer is more stable by over 10 kcal.mol^{-1}.

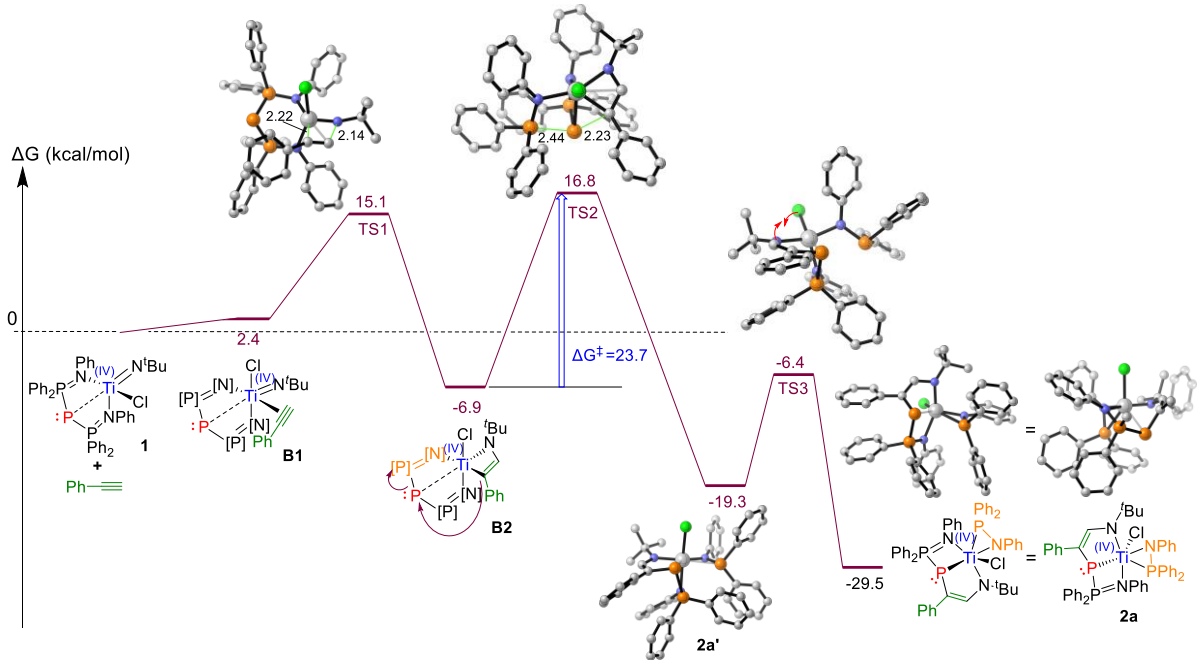

Figure 3. Most favorable computed mechanism (**B**) for the formation of **2a**.

As mentioned above, the Ti-P1 bond lengths in **2a-d** are indicative of the phosphide character of the NPN' ligand; Ti(IV) phosphide complexes are rare, due to the reducing nature of phosphides and the propensity of Ti(IV) to undergo one-electron reduction.[53] In order to strengthen the Ti-P1 interaction further, we abstracted the chloride ligand in **2a** with the triethylsilylium cation. An immediate color change from dark brown to deep red was observed, and complex **3** was isolated in 90 % yield after workup (Scheme 3).

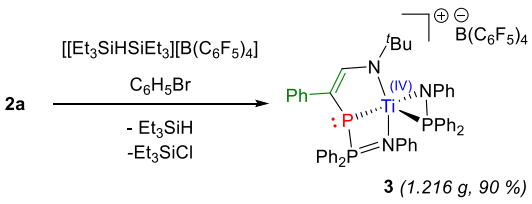

Scheme 3. Synthesis of **3**.

Chloride removal has a strong impact on the $^{31}P\{^{1}H\}$ NMR spectrum of **3** vs **2a** (Figure 4). All the signals are significantly broadened, to the extent that $^{2}J_{P1P3}$ and $^{3}J_{P2P3}$ coupling constants are no longer observed. Moreover, the signals now span a much narrower range of frequencies: 12.2 ppm *vs* 81.4 for **2a**. The signal for P1 is strongly deshielded compared to the one observed in **2a** (-8.8 *vs* -62.3 ppm). Interestingly however, it is very far from the 400-500 ppm values reached by other d^0 cationic Ti-phosphide complexes:[53] this is likely a consequence of the absence of multiple bond character for the Ti-P interaction (*vide infra*).[58]

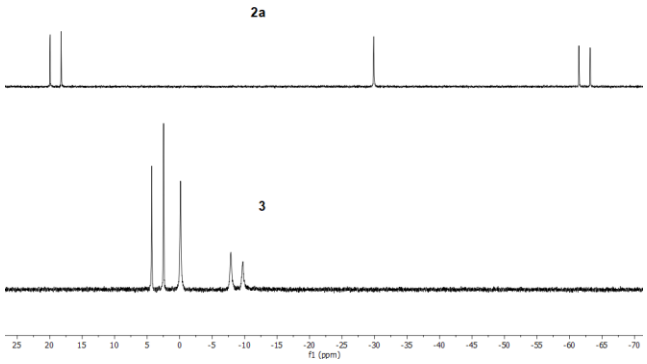

Figure 4. Comparison of the $^{31}P\{^{1}H\}$ NMR spectra of **2a** and **3** (CD_2Cl_2, 202 MHz).

X-ray diffraction analysis of a single crystal of **3** revealed the structure shown in Figure 5. Being both chiral at Ti and at P1, it also crystallizes as a single diastereomer.

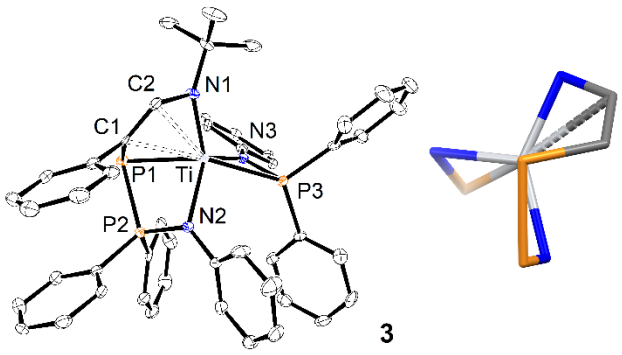

Figure 5. Left: ORTEP depiction of the X-ray structure of **3** (thermal ellipsoids drawn at the 50% probability level; solvent molecules, $B(C_6F_5)_4^-$ anion and hydrogen atoms are not shown for clarity). Selected bond distances (Å) and angles (°): C1-C2: 1.372(7); Ti-C1: 2.538(5); Ti-C2: 2.453(5); Ti-N1: 1.925(4); Ti-N2: 2.085(4); Ti-N3: 1.953(4); Ti-P1: 2.4767(16); Ti-P3: 2.4390(16); P1-P2: 2.1676(19); P2-N2: 1.633(4); P3-N3: 1.681(5); C1-P1-P2: 94.89(17); N1-Ti-N2: 139.47(17); Σα(P1): 240.2(2). Right: Capped sticks depiction of the first coordination sphere of Ti in **3** viewed along the Ti-P1 bond.

Except for the Ti-P3 distance, which remains the same as that observed in **2a**, all the distances between Ti and C, N and P atoms are shorter in **3** compared to **2a**. This is especially noticeable for the Ti-P1 distance (2.4767(16) Å *vs* 2.5496(6) Å). Additionally, the N1-Ti-N2 angle is narrower (139.47(17) ° *vs* 153.73(7) °), as well as the C1-P1-P2 angle (94.89(17) ° vs 101.90(7) °). Because of these increased geometrical constraints, the P1 atom is further pyramidalized (240.2(9) ° *vs* 251.58(10) °).

Complex **3** is a moderately active initiator for the ring-opening polymerization (ROP) of *rac*-lactide, converting 67 % of the monomer over 24h (toluene, 110 °C, 100 eq lactide, 1 eq benzyl alcohol). This level of performance is unexceptional for titanium, which tends to yield poorly active ROP initiators compared to other group 4 metals.[59, 60] Interestingly, however, the obtained polymer displays a slight heterotactic bias (Pm = 0.40).

We have previously shown that Ti(IV) cations containing a pendant phosphine ligand behave like Frustrated Lewis Pairs (FLP) towards aldehydes.[53, 61] Thus, we reacted **3** with 4-iodobenzaldehyde in CH_2Cl_2, and complex **4** was isolated in 70 % yield after workup (Scheme 4).

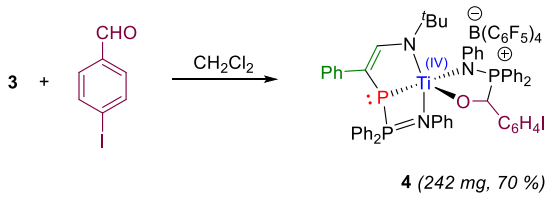

Scheme 4. Synthesis of **4**.

Initially, we ran the reaction for 5 minutes, and we observed a set of well-resolved signals (major product) along with another set of broad signals (minor product) in the $^{31}P\{^{1}H\}$ NMR spectrum of the isolated product (Figure S41). The chemical shifts of the minor product are very similar to the major product, suggestive of the presence of two different diastereomers. Running the reaction for 24 h afforded complex **4** as a single diastereomer, indicating that the minor diastereomer is a kinetic product.

Unfortunately, we were unable to obtain single crystals of **4** suitable for X-ray diffraction. However, the NMR spectroscopic data strongly suggest that the connectivity of **4** as depicted in Scheme 4 is correct. The $^{31}P\{^{1}H\}$ NMR spectrum of the major product features a strongly deshielded singlet at 70.5 ppm corresponding to the phosphonium (P3), a doublet at -6.6 ppm corresponding to the iminophosphoranyl (P2) and a doublet at -76.2 corresponding to the phosphide (P1). Both the chemical shifts of P1 and P2 and magnitude of the scalar coupling ($^{1}J_{P1P2}$ = 383 Hz) are roughly similar to those observed for **2a** (Figure 6), while the deshielding of the signal of P3 indicates that the amidophosphine ligand has reacted as the Lewis basic component of the FLP. This assumption is corroborated by the presence of a distinct cross-peak signal between P3 and the *ortho* protons of the 4-iodophenyl ring in the ^{1}H-^{31}P HMBC spectrum (Figure S47).[62]

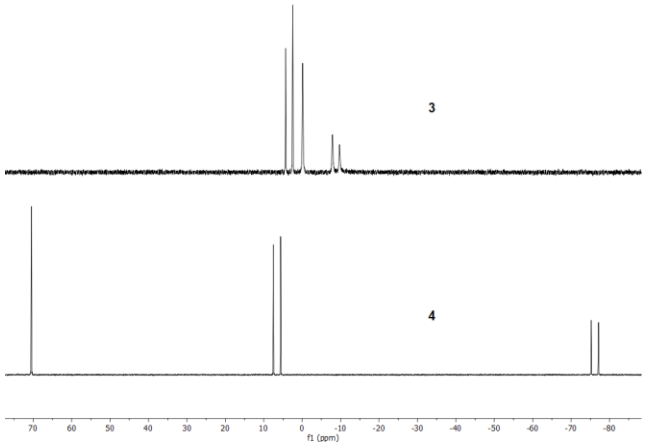

Figure 6. Comparison of the $^{31}P\{^{1}H\}$ NMR spectra of **3** and **4** (CD_2Cl_2, 202 MHz).

In another attempt to investigate the reactivity of **3**, we obtained a 1:1 mixture of **5** and **6** upon reaction with $SbCl_3$.[63] This mixture could be separated into its analytically pure constituents in 94 % and 54 % yields (respectively) after workup (Scheme 5).

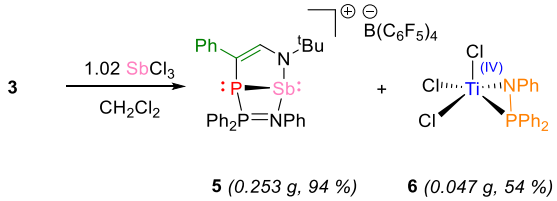

Scheme 5. Synthesis of **5** and **6**.

The $^{31}P\{^{1}H\}$ NMR spectrum of **5** features two doublets at 100.1 (P2) and -52.5 ppm (P1) with a $^{1}J_{P1P2}$ coupling constant of 306 Hz. The origin of the strong deshielding for P2 in **5** is unclear, since the bonding situation does not seem to differ drastically between Ti and Sb (*vide infra*). Other NMR parameters are comparable to those of other NPN'-containing compounds reported in this study (Table 1). For complex **6**, a singlet at -17.1 ppm is observed in the $^{31}P\{^{1}H\}$ NMR spectrum.

Single crystals of **5** and **6** suitable for X-ray diffraction analysis were obtained (see Figure 7; **5**: diffusion of pentane into a CH_2Cl_2 solution at -18 °C; **6**: saturated pentane solution at – 18°C). Strikingly, despite the considerably smaller covalent radius of Sb compared to Ti (1.39±0.05 Å vs

1.60±0.08 Å),[51] the M-N1, M-N2 and M-P1 distances are larger in **5** compared to **4** (Sb-N1: + 8 %; Sb-N2: + 1 %; Sb-P1: + 3 %). Other noticeable differences are the larger P1-P2 distance in **5** (+ 2 %), and the less pyramidalized P1 atom (-13 %), which also contribute to a more relaxed structure. Just like P1, the Sb atom displays a pyramidal geometry (Σα(Sb): 259.59(12) °), so that **5** could exist as two diastereomers — at least in principle. However, it is likely that inversion of either P1 or Sb would cause too much distortion to the bicyclic structure, so that only the diastereomer present in the crystal structure of **5** is observed.

Complex **6** displays a tetrahedral geometry (assuming that the amidophosphine ligand occupies one coordination site). The Ti-N and Ti-P distances (1.949(4) Å and 2.4294(15) Å, respectively) are slightly shorter than those observed in **2a-d**, consistent with a less crowded coordination environment in **6**.

It thus appears that the NPN' ligand in **3** can be transferred to Sb by transmetallation. We computed the thermodynamics of the reaction depicted in Scheme 5 by Density Functional Theory (DFT, see the supporting information for details) and indeed found a favorable reaction Gibbs free energy of -9.5 kcal.mol^{-1}. In an effort to investigate the generality of this transmetallation, we reacted **3** with other MCl_n precursors (PCl_3, $BiCl_3$, $ZrCl_4$, and K_2PdCl_6) in CD_2Cl_2, but we only obtained complex mixtures (Figure S68).

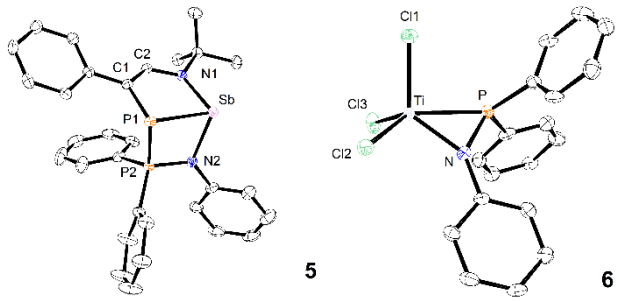

Figure 7. ORTEP depiction of the X-ray structures of **5** and **6** (thermal ellipsoids drawn at the 50% probability level; solvent molecules, $B(C_6F_5)_4^-$ anion and hydrogen atoms are not shown for

clarity). Selected bond distances (Å) and angles (°) for **5**: C1-C2: 1.367(3); Sb-N1: 2.070(2); Sb-N2: 2.101(2); Sb-P1: 2.5508(7); P1-P2: 2.2196(9); P2-N2: 1.646(2); C1-P1-P2: 99.52(8); N1-Sb-N2: 99.86(8); Σα(P1): 271.59(12); Σα(Sb): 259.56(12). Selected bond distances (Å) and angles (°) for **6**: Ti-Cl1: 2.2433(15); Ti-Cl2: 2.2404(15); Ti-Cl3:2.2053(15); Ti-N: 1.949(4); Ti-P: 2.4294(15); Cl1-Ti-Cl2: 102.32(6); Cl2-Ti-Cl3: 109.09(6); Cl3-Ti-Cl1: 110.85(7); Σα(N): 359.6(5).

Bonding analysis

In order to elucidate the electronic structure of **3** and **5**, we optimized the corresponding cations with DFT in dichloromethane (see the computational details). The computed geometries of $\mathbf{3}^+$ and $\mathbf{5}^+$ are in good agreement with the experimental X-ray diffraction structures, for instance the Ti-P and Sb-P bonds are well reproduced (2.52 Å and 2.60 Å, respectively *vs* 2.48 Å and 2.55 Å for the experimental values).

The bonding situation in $\mathbf{3}^+$ and $\mathbf{5}^+$ was analyzed using Bader's Atoms in Molecules (AIM).[64-66] The corresponding contour maps of the Laplacian of the electronic density are shown in Figure 8. Interestingly, the NPN' ligand retains a normal covalent P-P bond like the BIPP ligand: indeed, the topological parameters at the bond critical point (Table 3) and the aspect of the contour map of $\nabla^2\rho$ in the region of the P-P bond (Figure 8) are similar between **1**,[24] $\mathbf{3}^+$ and $\mathbf{5}^+$. A slightly less negative value of $\nabla^2\rho$ is observed at the bond critical point for $\mathbf{3}^+$ and $\mathbf{5}^+$ (-4.29 e Å^{-5} and -3.78 e Å^{-5}, respectively, *vs* -4.46 e Å^{-5} on average for **1**), pointing to a slightly more polar P-P bond in the NPN' ligand. Within the latter, the P1-C1 bond is even more polarized than the P1-P2 bond, as evidenced by the small charge depletion ($\nabla^2\rho > 0$) at the bond critical point.

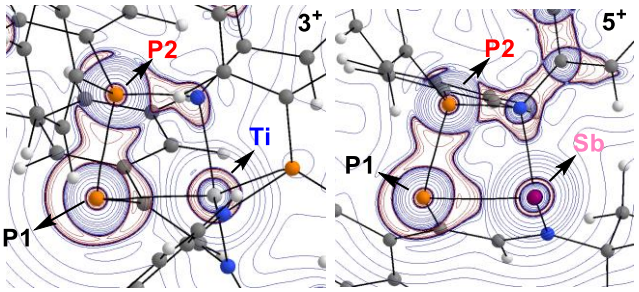

Figure 8. Contour maps of $\nabla^2\rho$ in the M–P–P plane for $\mathbf{3}^+$ (left) and $\mathbf{5}^+$ (right); red lines indicate charge concentration and blue lines indicate charge depletion.

Another interesting feature of the NPN' ligand is the similarity between M-N bonds in $\mathbf{3}^+$ and $\mathbf{5}^+$: indeed, following the classification rules set by Macchi and Sironi, these bonds display the characteristics of both a polarized covalent bond between light atoms (large ρ; $G/\rho \geq 1$) and a donor-acceptor interaction between heavy atoms ($\nabla^2\rho > 0$; $H/\rho < 0$) .[67, 68] This intermediate bonding situation is consistent with the participation of an atom with 4 (Ti) or 5 (Sb) atomic shells in the M-N bond. Thus, although the M-N2 bonds are slightly more polar than the M-N1 and Ti-N3 bonds (less positive $\nabla^2\rho$, lower DI), iminophosphorane and amide ligands share common characteristics. This is consistent with the notion that the zwitterionic representation of iminophosphoranes (P^+–N^-) should be favored over the hypervalent "ene" form (P=N).[69]

Table 3. Relevant AIM topological indexes for $\mathbf{3}^+$ and $\mathbf{5}^+$.

		ρ (e Å^{-3})	$\nabla^2\rho$ (e Å^{-5})	G/ρ (E_h e^{-1})	H/ρ (E_h e^{-1})	DI
$\mathbf{3}^+$	P1-P2	0.80	-4.29	0.26	-0.63	0.89
	P1-C1	0.97	2.46	1.01	-0.84	0.96
	Ti-N1	0.86	10.53	1.20	-0.34	0.83
	Ti-N2	0.62	7.30	1.04	-0.21	0.53
	Ti-N3	0.82	9.33	1.12	-0.33	0.75

	Ti-P1	0.43	1.25	0.47	-0.26	0.56
	Ti-P3	0.36	2.96	0.76	-0.18	0.34
5^+	P1-P2	0.77	-3.78	0.22	-0.57	0.82
	P1-C1	1.04	1.78	0.99	-0.87	0.97
	Sb-N1	0.67	6.96	1.00	-0.27	0.79
	Sb-N2	0.59	6.19	0.97	-0.24	0.72
	Sb-P1	0.49	-0.10	0.32	-0.34	0.82

Despite the similarities between $\mathbf{3}^+$ and $\mathbf{5}^+$, these compounds differ slightly where the M-P1 interaction is concerned. The Sb-P1 bond displays the characteristics of a normal covalent bond (*e.g.* $G/\rho < 1$), which are actually not too dissimilar from those of the P1-P2 bond. Obviously, the presence of a heavy element does change the topology of $\nabla^2\rho$ in the region of the Sb-P bond, but the resemblance is still visible (Figure 8, right).

The Ti-P1 bond, on the other hand, is much more polarized towards P, as expected from the electronegativity difference between these elements:[70] this is evident in the slightly positive value of $\nabla^2\rho$ (1.25 e Å^{-5}) at the bond critical point, in the low delocalization index (DI = 0.56), and in the contour map of $\nabla^2\rho$ (Figure 8, left).[71] Importantly, the Ti-P3 interaction (which chemical common sense urges to describe as a donor-acceptor interaction despite the values in Table 3) displays similar characteristics as Ti-P1.

These conclusions are in agreement with the topological analysis of ELF basins shown in Figure 9. Indeed, the V(P1,P2) bonding basin is present in both complexes, consistent with a normal covalent P-P bond. Moreover, the ELF analysis also indicates that the donor-acceptor character of the M-N and M-P bonds is more pronounced with Ti than with Sb. Thus, V(N1, Sb) and V(N2, Sb) bonding basins can be observed in $\mathbf{5}^+$ (instead of lone pairs on N1 and N2 in $\mathbf{3}^+$), while one of

the lone pairs on P1 is on the verge of becoming a V(P1, Sb) bonding basin. Finally, the diffuse lone pair on Sb is clearly visible.

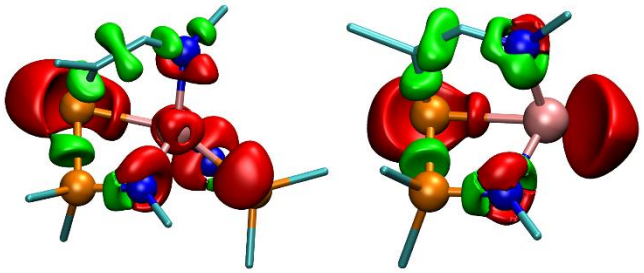

3^+ 5^+

Figure 9. ELF basins of $\mathbf{3}^+$ and $\mathbf{5}^+$ limited to the first coordination sphere of the metal. Red volumes indicate lone pairs and green volumes indicate bonding basins.

To summarize the results of these topological analyses of the bonding situation in $\mathbf{3}^+$ and $\mathbf{5}^+$, we propose the Lewis representations depicted in Chart 5.

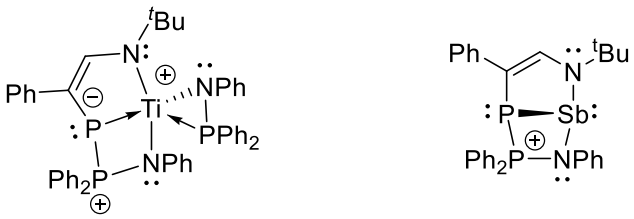

3^+ 5^+

Chart 5. Suggested Lewis representation for $\mathbf{3}^+$ and $\mathbf{5}^+$ according to AIM analysis.

Conclusion

The reactivity of dicoordinate phosphorus compounds has long been recognized as a useful synthetic tool, providing access to a variety of "P^+" synthons with controlled reactivity. In the herein reported study, we have shown that a Ti-coordinated BIPP ligand undergoes nucleophilic cleavage of one of its P-P bonds. These ligands can therefore be considered a new addition to the small family of *ambiphilic phosphides*. The reactivity of complex **1** towards alkynes results in the template formation of highly functionalized NPN' ligands that would otherwise be extremely

difficult (if not impossible) to synthesize. We are currently investigating further rearrangements enabled by the residual ambiphilic character of the NPN' ligand.

Experimental section

General considerations

All reactions were carried out under Ar using conventional Schlenk techniques or in an Ar glovebox. Toluene, CH_2Cl_2, Et_2O, pentane and THF were dried using an MBraun MB SPS-800 solvent purification system. Bromobenzene was distilled over CaH_2 and stored over activated 3Å molecular sieves in the glovebox. Deuterated solvents and terminal alkynes were dried by passage through a short column of activated neutral alumina (Brockman grade II). Additionally, deuterated solvents were stored over activated 3Å molecular sieves in the glovebox, either at room temperature (C_6D_6, C_6D_5Br…) or at -18°C (d_8-THF, CD_2Cl_2…). Alumina and molecular sieves were activated by heating for at least 6 hours above 230°C under vacuum. Diatomaceous earth (dicalite) was dried in an oven at 110 °C. Complex **1**[24] and $[Et_3SiHSiEt_3][B(C_6F_5)_4]$[72] were prepared according to literature procedures. All other reagents were commercially available and used as received.

For analytical details (including NMR spectroscopic data for compounds **2a-d** and **3-6**), kinetic studies and additional reactivity experiments, see the Supporting Information.

Synthesis of compounds

2a. In an Ar glovebox, complex **1** (1.63 g, 1.96 mmol) and phenylacetylene (930 mg, 7.79 mmol) were dissolved in CH_2Cl_2. The reaction mixture was stirred for two days and three nights, filtered over a borosilicate fibre filter, then evaporated to dryness. The solid residue was triturated in 50 mL of pentane and the suspension was filtered over a sintered glass frit. The resulting solid was rinsed with pentane and dried under vacuum, yielding complex **2a** as a purple-brown powder

(1.323 g, 79 %). Single crystals suitable for X-ray diffraction were grown by slow diffusion of pentane into a CH_2Cl_2 solution of **2a** at -20 °C. **Elemental Analysis:** calculated for $C_{48}H_{45}ClN_3P_3Ti$: C, 68.62; H, 5.40; N, 5.00. Found: C, 68.59; H, 5.42; N, 4.95.

2b. In an Ar glovebox, complex **1** (415 mg, 0.05 mmol) and valylene (210 mg, 3.18 mmol) were dissolved in CH_2Cl_2. The reaction mixture was stirred for 7 days, filtered over a borosilicate fibre filter, then evaporated to dryness. The solid residue was triturated in 10 mL of pentane and the suspension was filtered over a sintered glass frit. The resulting solid was rinsed with pentane and dried under vacuum, yielding complex **2b** as a green-brown powder (308 mg, 77%). Elemental analysis was performed on a batch recrystallized from CH_2Cl_2/pentane (Figure S16).

Elemental Analysis: calculated for $C_{45}H_{45}ClN_3P_3Ti$: C, 67.22; H, 5.64; N, 5.23. Found: C, 67.54; H, 5.73; N, 5.25.

2c. In an Ar glovebox, complex **1** (1 g, 1.2 mmol, 1 eq) and cyclopropylacetylene (405 mg, 6 mmol, 5 eq) were mixed in CH_2Cl_2. The reaction mixture was stirred for eleven days, filtered over a borosilicate fibre filter, then evaporated to dryness. The solid residue was triturated in 20 mL of pentane and the suspension was filtered over a sintered glass frit. The resulting solid was rinsed with pentane and dried under vacuum, yielding complex **2c** as a brown powder (800 mg, 91%). Elemental analysis was performed on a batch of compound containing 10 mol% of pentane and 30 mol% of CH_2Cl_2, respectively (see figure S24). **Elemental Analysis:** calculated for $C_{45}H_{45}ClN_3P_3Ti(C_5H_{12})_{0.10}(CH_2Cl_2)_{0.3}$: C, 65.74; H, 5.64; N, 5.02. Found: C, 65.91; H, 6.01; N, 5.07.

2d. In an Ar glovebox, complex **1** (1.157 g, 1.4 mmol, 1 eq) and 2-ethynylpyridine (744 mg, 7 mmol, 5 eq) were mixed in CH_2Cl_2. The reaction mixture was stirred for 10h, filtered over a borosilicate fibre filter, then evaporated to dryness. The solid residue was triturated in 50 mL of pentane and the suspension was filtered over a sintered glass frit. The resulting solid was rinsed

with pentane and dried under vacuum, yielding complex **2d** as a dark brown powder (1.165 g, 99%). Elemental analysis was performed on a batch of compound containing 10 mol% of pentane (see figure S32). **Elemental Analysis:** calculated for $C_{47}H_{44}ClN_4P_3Ti(C_5H_{12})_{0.1}$: C, 67.25; H, 5.37; N, 6.60. Found: C, 66.96; H, 5.81; N, 6.78.

3. *Note: this synthesis was performed using Apiezon H grease in order to avoid the formation of Ti-polysiloxane adducts.* In an Ar glovebox, complex **2a** (750 mg, 0.89 mmol) and $[Et_3SiHSiEt_3][B(C_6F_5)_4]$ (813 mg, 0.89 mmol) were dissolved in C_6H_5Br in a 20 mL crimp seal vial. The reaction mixture was stirred for 5 min. It was then added to 80 mL of pentane under vigorous agitation in a Schlenk flask and stirred for 1 h, during which a brown-red solid formed on the walls of the Schlenk. The supernatant was discarded, the solid was crushed and suspended in 30 mL of pentane. The suspension was filtered over a sintered glass frit, and the resulting solid was rinsed with pentane (10 mL) and dried on the frit, yielding complex **3** as a red-brown powder containing 25mol% of pentane (1.216 g, 90 %). Single crystals suitable for X-ray diffraction were grown by slow diffusion of pentane into a CH_2Cl_2 solution of **3** at -20 °C. **Elemental Analysis:** calculated for $C_{72}H_{45}BF_{20}N_3P_3Ti(C_5H_{12})_{0.25}$: C, 58.28; H, 3.22; N, 2.80. Found: C, 57.51; H, 2.34; N, 2.64. **HRMS (ESI-pos):** calculated for $C_{48}H_{45}N_3P_3Ti^+$ $[M\text{-}B(C_6F_5)_4]^+$: 804.23003. Found: 804.22871 (-1.6 ppm).

4. In an Ar glovebox, complex **3** (304 mg, 0.2 mmol) and *p*-iodo benzaldehyde (46.4 mg, 0.2 mmol) were dissolved in CH_2Cl_2 (1.5 mL), affording a greenish-brown solution instantly. Work-up at this stage gives complex **4** as a mixture of two diastereomers (see Figure S41). The reaction mixture was stirred for 24 h, then added to 120 mL of pentane under vigorous stirring. A brown solid precipitated, which was filtered over a sintered glass fritt. The solid was suspended twice in 20 mL of pentane and dried under vacuum, affording complex **4** as a greenish-brown powder containing 20 % of pentane (242 mg, 70 %) and over 95 % of the major diastereoisomer.

Elemental Analysis: calculated for $C_{79}H_{50}BF_{20}IN_3OP_3Ti(C_5H_{12})_{0.2}$: C, 55.54; H, 3.45; N, 2.03. Found: C, 55.26; H, 3.46; N, 2.52.

5 and **6**. In an Ar glovebox, complex **3** (304 mg, 0.20 mmol) and $SbCl_3$ (48 mg, 0.21 mmol) were dissolved in CH_2Cl_2 (3 mL) in a 20 mL crimp seal vial. The reaction mixture was stirred overnight, and was layered with 15 mL of pentane. A solid precipitated, which was filtered over a sintered glass frit, and suspended four times in 5 mL of pentane. After drying on the frit, complex **5** was obtained as a brick-red solid containing 50 mol% of CH_2Cl_2 and 50 mol% of pentane (0.253 g, 94 %). Prolonged drying afforded pentane-free material suitable for analyses. The filtrate was concentrated under vacuum and stored in a 20 mL crimp seal vial at -20 °C. Red crystals grew overnight, the supernatant solution was discarded and the crystals were crushed. Complex **6** was obtained as a red powder (0.047 g, 54 %). Single crystals suitable for X-ray diffraction analysis were obtained by slow diffusion of pentane into a CH_2Cl_2 solution of **5** at -20 °C. For **6**, crystals were obtained by cooling a saturated solution of **6** in pentane at -20°C. **Elemental Analysis of 5:** calculated for $C_{54}H_{30}BF_{20}N_2P_2Sb(CH_2Cl_2)_{0.5}$: C, 49.45; H, 2.36; N, 2.80. Found: C, 50.33; H, 2.43; N, 2.10. **Elemental Analysis of 6:** calculated for $C_{18}H_{15}Cl_3NPTi$: C, 50.22; H, 3.51; N, 3.25. Found: C, 50.02; H, 3.57; N, 3.33.

Computational details

All Quantum mechanics calculations were performed using the Gaussian 16 package.[73] Energy and forces were computed by density functional theory with the hybrid B3LYP exchange-correlation functional.[74-77] The dichloromethane solvent effects were modelled by means of the continuum model within the SMD approach as implemented in Gaussian.[78] In addition, dispersion effects have been considered using the D3 dispersion correction suggested by Grimme et al. with Becke-Johnson damping.[79] Geometries were optimized and characterized with the double-z quality plus polarization def2-SVP basis set.[80] Transition states were localized using the string

theory[E, W.; Ren, W.; Vanden-Eijnden, E. *Phys. Rev. B: Condens. Matter Mater. Phys.* **2002**, *66*, 052301] as implemented in Opt'n Path.[81] Gibbs free energies have been computed at 298 K and 1 atm using unscaled density functional frequencies.

In order to gain insight into the nature of the chemical bonding, we performed Atoms In Molecules analysis (QTAIM),[64, 82] using AIMALL software,[83] and Electron Localization Function analysis using the TopChem2 package.[84, 85] The ELF basins have been plotted with VMD software.[86, 87] 3D geometries have been drawn with CYLview.[88]

ASSOCIATED CONTENT

Supporting Information. The Supporting Information is available free of charge on the ACS Publications website at DOI: 10.1021/acs.inorgchem.xxxxxxx Supporting Information: full experimental details and analyses for compounds **2a-d**, **3**, **4**, **5**, **6** ; additional computational analyses (ELF, AIM) and structures of $\mathbf{3}^{+}$ and $\mathbf{5}^{+}$; theoretical free energy profile for pathway A; crystallographic tables (PDF). CCDC 2122693 (**2a**), 2122694 (**2b**), 2122695 (**2c**), 2122696 (**2d**), 2122697 (**3**), 2122698 (**5**), 2122699 (**6)** contain the supplementary crystallographic data for this paper. These data can be obtained free of charge from The Cambridge Crystallographic Data Centre. Cartesian coordinates and free energies of all computed structures are given in a separate X-mol file.

AUTHOR INFORMATION

Corresponding Author

Dr Adrien T. Normand* Institut de Chimie Moléculaire de l'Université de Bourgogne, UMR 6302, Université de Bourgogne, 9 avenue Alain Savary 21000 Dijon (FR). Email: adrien.normand@u-bourgogne.fr; ORCID: 0000-0002-8047-9386.

Prof Paul Fleurat-Lessard* Institut de Chimie Moléculaire de l'Université de Bourgogne, UMR 6302, Université de Bourgogne, 9 avenue Alain Savary 21000 Dijon (FR). Email: Paul.fleurat-lessard@u-bourgogne.fr; ORCID: 0000-0003-3114-2522.

Author Contributions

The manuscript was written through contributions of all authors. All authors have given approval to the final version of the manuscript.

Funding Sources

Financial support from CNRS, UB, Conseil Régional de Bourgogne Franche-Comté (PhosFerTiMn, PARI CDEA), FEDER and the PIA-excellence ISITEBFC program (COMICS) is gratefully acknowledged. Calculations were performed partly using HPC resources from DNUM CCUB (Centre de Calcul de l'Université de Bourgogne). This work was also granted access to the HPC resources of CINES under the allocation A0090807259 made by GENCI.

Notes

The authors declare no competing financial interest.

ACKNOWLEDGMENT

We are indebted to Dr Philippe Richard (who also solved the crystal structure of **2a**) for an enlightening discussion about centrosymmetric crystallographic groups. We thank Dr Quentin Bonnin and Ms Marie-José Penouilh-Suzette (PACSMUB) for technical assistance with NMR spectroscopy, and performing ESI-MS analysis. Mr Marcel Soustelle and Ms Tiffanie Régnier (PACSMUB) performed elemental analysis.

REFERENCES

1. Cowley, A. H.; Kemp, R. A. Synthesis and reaction chemistry of stable two-coordinate phosphorus cations (phosphenium ions). *Chem. Rev.* **1985,** *85*, 367-382.
2. Lochschmidt, S.; Schmidpeter, A. Die chemische verschiebung des zweifachkoodinierten phosphors, I. *Phosphorus and Sulfur and the Related Elements* **1986,** *29*, 73-109.
3. Gudat, D. Cationic low coordinated phosphorus compounds as ligands: Recent developments. *Coord. Chem. Rev.* **1997,** *163*, 71-106.
4. Marque, S.; Tordo, P. In *New Aspects in Phosphorus Chemistry V*; Majoral, J.-P., Ed.; Springer Berlin Heidelberg: 2005; Chapter 2, Vol. 250, pp 43-76.
5. Issleib, K.; Döll, G. Alkali-Phosphorverbindungen und ihr reaktives Verhalten, XX. Äthylen-1.2-bis-monocyclohexylphosphin und -monoäthylphosphin. *Chem. Ber.* **1963,** *96*, 1544-1550.
6. Issleib, K.; Häckert, H. Cyclopentadienyl-Metallphosphide des Titan(III) und Zirkon(III). *Z. Naturforsch. B* **1966,** *21*, 519-521.
7. Ishida, S.; Hirakawa, F.; Iwamoto, T. A Stable Dialkylphosphinyl Radical. *J. Am. Chem. Soc.* **2011,** *133*, 12968-12971.
8. Hirakawa, F.; Ichikawa, H.; Ishida, S.; Iwamoto, T. Redox Reactions of a Stable Dialkylphosphinyl Radical. *Organometallics* **2015,** *34*, 2714-2716.
9. Olaru, M.; Mischin, A.; Malaspina, L. A.; Mebs, S.; Beckmann, J. The Bis(ferrocenyl)phosphenium Ion Revisited. *Angew. Chem. Int. Ed.* **2020,** *59*, 1581-1584.
10. Olaru, M.; Mebs, S.; Beckmann, J. Cationic Carbene Analogues: Donor-Free Phosphenium and Arsenium Ions. *Angew. Chem. Int. Ed.* **2021,** *60*, 19133-19138.
11. Stalder, T.; Krischer, F.; Steinert, H.; Neigenfind, P.; Gessner, V. H. Ylide-Stabilized Phosphenium Cations: Impact of the Substitution Pattern on the Coordination Chemistry. *Chem. Eur. J.* **2022,** *28*, e202104074.
12. Schmidpeter, A.; Zwaschka, F. Dicynophosphide. *Angew. Chem. Int. Ed.* **1977,** *16*, 704-705.
13. Schmidpeter, A.; Bürget, G. Dicyanphosphid-Reaktionen. *Z. Naturforsch. B* **1985,** *40*, 1306.
14. Binder, J. F.; Kosnik, S. C.; St Onge, P. B. J.; Macdonald, C. L. B. Synthesis of Heavy Dicyanamide Homologues from Air-Stable Precursors. *Chem. Eur. J.* **2018,** *24*, 14644-14648.
15. Sacher, W.; Schmidpeter, A.; Beck, W. Organometallic Lewis Acids, Part LIX Pentacarbonylrhenium Complexes with Phosphorus Tricyanide and Di-cyanophosphide. *Zeit. Anorg. Allg. Chem.* **2015,** *641*, 762-764.
16. Hardman, N. J.; Abrams, M. B.; Pribisko, M. A.; Gilbert, T. M.; Martin, R. L.; Kubas, G. J.; Baker, R. T. Molecular and Electronic Structure of Platinum Bis(N-arylamino)phosphenium Complexes including [Pt(phosphane)(phosphenium)(N-heterocyclic carbene)]. *Angew. Chem. Int. Ed.* **2004,** *43*, 1955-1958.
17. Gudat, D.; Schrott, M.; Bajorat, V.; Nieger, M. Bis(Phosphonio)-Isophosphindolium Cations as Ligands in Coordination Chemistry: Anionic Behaviour of Cationic Species. *Phosphorus, Sulfur, Silicon Relat. Elem.* **1996,** *109*, 125-128.
18. Gudat, D.; Schrott, M.; Nieger, M. A novel coordination mode for cationic phosphorus pπ systems: μ2-bridging coordination of a bis(phosphonio)isophosphindolium cation. *J. Chem. Soc. Chem. Commun.* **1995**, 1541-1542.

19. Gudat, D.; Schrott, M.; Bajorat, V.; Nieger, M.; Kotila, S.; Fleischer, R.; Stalke, D. [Bis(phosphonio)isophosphindolide]silver Complexes. *Chem. Ber.* **1996,** *129*, 337-345.
20. Schmidpeter, A.; Thiele, M. Diphosphonio Isophosphindoles, Phospholes with a Planar Phosphorus. *Angew. Chem. Int. Ed.* **1991,** *30*, 308-310.
21. Sarbajna, A.; Swamy, V. S. V. S. N.; Gessner, V. H. Phosphorus-ylides: powerful substituents for the stabilization of reactive main group compounds. *Chem. Sci.* **2021,** *12*, 2016-2024.
22. Chong, C. C.; Rao, B.; Ganguly, R.; Li, Y.; Kinjo, R. Bis(N-heterocyclic olefin) Derivative: An Efficient Precursor for Isophosphindolylium Species. *Inorg. Chem.* **2017,** *56*, 8608-8614.
23. Normand, A. T.; Sosa Carrizo, E. D.; Magnoux, C.; Lobato, E.; Cattey, H.; Richard, P.; Brandès, S.; Devillers, C. H.; Romieu, A.; Le Gendre, P.; Fleurat-Lessard, P. Reappraising Schmidpeter's bis(iminophosphoranyl)phosphides: coordination to transition metals and bonding analysis. *Chem. Sci.* **2021,** *12*, 253-269.
24. Cantat, T.; Mezailles, N.; Auffrant, A.; Le Floch, P. Bis-phosphorus stabilised carbene complexes. *Dalton Trans.* **2008**, 1957-1972.
25. Fustier-Boutignon, M.; Nebra, N.; Mézailles, N. Geminal Dianions Stabilized by Main Group Elements. *Chem. Rev.* **2019,** *119*, 8555-8700.
26. the ene form (P=C) is "chemically wrong", but it is much more legible than the charge-laden, octet-rule abiding ylidic form (P^{+}-C^{-}), therefore we use the former throughout this paper. The same goes for the iminophosphoranyl group.
27. Ellis, B. D.; Macdonald, C. L. B. Stable compounds containing heavier group 15 elements in the +1 oxidation state. *Coord. Chem. Rev.* **2007,** *251*, 936-973.
28. Coffer, P. K.; Dillon, K. B. Cyclic triphosphenium ions and related species. *Coord. Chem. Rev.* **2013,** *257*, 910-923.
29. Dionisi, E. M.; Binder, J. F.; LaFortune, J. H. W.; Macdonald, C. L. B. Triphosphenium salts: air-stable precursors for phosphorus(I) chemistry. *Dalton Trans.* **2020,** *49*, 12115-12127.
30. However, it should be emphasized that the P-P bonds in both classes of compounds are normal covalent, not dative (see ref 24).
31. Ellis, B. D.; Dyker, C. A.; Decken, A.; Macdonald, C. L. B. The synthesis, characterisation and electronic structure of N-heterocyclic carbene adducts of P^{I} cations. *Chem. Commun.* **2005**, 1965-1967.
32. Dube, J. W.; Macdonald, C. L. B.; Ragogna, P. J. Accessing the Coordination Chemistry of Phosphorus(I) Zwitterions. *Angew. Chem. Int. Ed.* **2012,** *51*, 13026-13030.
33. Dube, J. W.; Macdonald, C. L. B.; Ellis, B. D.; Ragogna, P. J. Synthesis of Zwitterionic Triphosphenium Transition Metal Complexes: A Boron Atom Makes The Difference. *Inorg. Chem.* **2013,** *52*, 11438-11449.
34. Kosnik, S. C.; Farrar, G. J.; Norton, E. L.; Cooper, B. F. T.; Ellis, B. D.; Macdonald, C. L. B. Low-Valent Chemistry: An Alternative Approach to Phosphorus-Containing Oligomers. *Inorg. Chem.* **2014,** *53*, 13061-13069.
35. Binder, J. F.; Swidan, A. a.; Tang, M.; Nguyen, J. H.; Macdonald, C. L. B. Remarkably stable chelating bis-N-heterocyclic carbene adducts of phosphorus(I) cations. *Chem. Commun.* **2015,** *51*, 7741-7744.
36. Kosnik, S. C.; Macdonald, C. L. B. A zwitterionic triphosphenium compound as a tunable multifunctional donor. *Dalton Trans.* **2016,** *45*, 6251-6258.

37. Macdonald, C. L. B.; Binder, J. F.; Swidan, A. a.; Nguyen, J. H.; Kosnik, S. C.; Ellis, B. D. Convenient Preparation and Detailed Analysis of a Series of NHC-Stabilized Phosphorus(I) Dyes and Their Derivatives. *Inorg. Chem.* **2016,** *55*, 7152-7166.
38. Kosnik, S. C.; Nascimento, M. C.; Binder, J. F.; Macdonald, C. L. B. Accessing multimetallic complexes with a phosphorus(I) zwitterion. *Dalton Trans.* **2017,** *46*, 17080-17092.
39. Binder, J. F.; Kosnik, S. C.; Macdonald, C. L. B. Assessing the Ligand Properties of NHC-Stabilised Phosphorus(I) Cations. *Chem. Eur. J.* **2018,** *24*, 3556-3565.
40. Binder, J. F.; Swidan, A. a.; Macdonald, C. L. B. Synthesis of Heteroleptic Phosphorus(I) Cations by P+ Transfer. *Inorg. Chem.* **2018,** *57*, 11717-11725.
41. Johnson, J. S.; Bergman, R. G. Imidotitanium Complexes as Hydroamination Catalysts: Substantially Enhanced Reactivity from an Unexpected Cyclopentadienide/Amide Ligand Exchange. *J. Am. Chem. Soc.* **2001,** *123*, 2923-2924.
42. Bytschkov, I.; Doye, S. Group-IV Metal Complexes as Hydroamination Catalysts. *Eur. J. Org. Chem.* **2003**, 935-946.
43. Müller, T. E.; Hultzsch, K. C.; Yus, M.; Foubelo, F.; Tada, M. Hydroamination: Direct Addition of Amines to Alkenes and Alkynes. *Chem. Rev.* **2008,** *108*, 3795-3892.
44. Kawakita, K.; Parker, B. F.; Kakiuchi, Y.; Tsurugi, H.; Mashima, K.; Arnold, J.; Tonks, I. A. Reactivity of terminal imido complexes of group 4–6 metals: Stoichiometric and catalytic reactions involving cycloaddition with unsaturated organic molecules. *Coord. Chem. Rev.* **2020,** *407*, 213118.
45. Manßen, M.; Schafer, L. L. Titanium catalysis for the synthesis of fine chemicals – development and trends. *Chem. Soc. Rev.* **2020,** *49*, 6947-6994.
46. Walsh, P. J.; Hollander, F. J.; Bergman, R. G. Generation, alkyne cycloaddition, arene carbon-hydrogen activation, nitrogen-hydrogen activation and dative ligand trapping reactions of the first monomeric imidozirconocene (Cp_2Zr=NR) complexes. *J. Am. Chem. Soc.* **1988,** *110*, 8729-8731.
47. Two nearly identical independent molecules were present in the cell for **2d**. We only discuss **2d-1**.
48. Dutartre, M.; Bayardon, J.; Juge, S. Applications and stereoselective syntheses of P-chirogenic phosphorus compounds. *Chem. Soc. Rev.* **2016,** *45*, 5771-5794.
49. **2a**, **2c** and **2d** crystallize in the P-1 group, while **2b** crystallizes in the P21/n group. These two groups are centrosymmetric, therefore two enantiomers are present in the cell for **2a-d**.
50. incidentally, **2d-1** and **2d-2** display opposite configurations, but they are not enantiomers because of slightly different metric parameters.
51. Cordero, B.; Gomez, V.; Platero-Prats, A. E.; Reves, M.; Echeverria, J.; Cremades, E.; Barragan, F.; Alvarez, S. Covalent radii revisited. *Dalton Trans.* **2008**, 2832-2838.
52. Rosenberg, L. Metal complexes of planar PR_2 ligands: Examining the carbene analogy. *Coord. Chem. Rev.* **2012,** *256*, 606-626.
53. Normand, A. T.; Bonnin, Q.; Brandès, S.; Richard, P.; Fleurat-Lessard, P.; Devillers, C. H.; Balan, C.; Le Gendre, P.; Kehr, G.; Erker, G. The Taming of Redox-Labile Phosphidotitanocene Cations. *Chem. Eur. J.* **2019,** *25*, 2803-2815.
54. an anonymous referee suggested a third mechanism in which the alkyne is activated by complex **2** following an FLP mechanism. We found that this is mechanism is highly unlikely given the instability of the resulting intermediate (C1, Figure S74). Yet another mechanism could be predicated upon the phosphenium character of the BIPP ligand in **1**. Indeed, phosphenium cations are known to undergo [2+1] cycloaddition with alkynes, yielding phosphirenium salts. However, this reaction only occurs with electron-deficient phospheniums, not ambiphilic

phosphides such as TP. See a) Fongers, K. S.; Hogeveen, H.; Kingma, R. F. Synthesis of phosphirenium salts. *Tetrahedron Lett.* **1983**, *24*, 643-646; b) Breslow, R.; Deuring, L. A. Concerning phosphirenium cations. *Tetrahedron Lett.* **1984**, *25*, 1345-1348.
55. Marinetti, A.; Mathey, F.; Fischer, J.; Mitschler, A. Generation and trapping of terminal phosphinidene complexes. Synthesis and x-ray crystal structure of stable phosphirene complexes. *J. Am. Chem. Soc.* **1982,** *104*, 4484-4485.
56. Marinetti, A.; Mathey, F. The chemistry of free and complexed phosphirenes: reactivity toward electrophiles, nucleophiles, and conjugated dienes. *J. Am. Chem. Soc.* **1985,** *107*, 4700-4706.
57. This value is in fair agreement with the experimental results. Indeed, applying the Eyring equation with a transmission coefficient of 1, the computed free energy barrier corresponds to a value of $k = 2.58. \times 10^{-4}\ s^{-1}$ (experimental value : $2.89 \times 10^{-4}\ s^{-1}$).
58. Halbert, S.; Copéret, C.; Raynaud, C.; Eisenstein, O. Elucidating the Link between NMR Chemical Shifts and Electronic Structure in d^0 Olefin Metathesis Catalysts. *J. Am. Chem. Soc.* **2016,** *138*, 2261-2272.
59. Le Roux, E. Recent advances on tailor-made titanium catalysts for biopolymer synthesis. *Coord. Chem. Rev.* **2016,** *306*, 65-85.
60. Sauer, A.; Kapelski, A.; Fliedel, C.; Dagorne, S.; Kol, M.; Okuda, J. Structurally well-defined group 4 metal complexes as initiators for the ring-opening polymerization of lactide monomers. *Dalton Trans.* **2013,** *42*, 9007-9023.
61. Normand, A. T.; Richard, P.; Balan, C.; Daniliuc, C. G.; Kehr, G.; Erker, G.; Le Gendre, P. Synthetic Endeavors toward Titanium Based Frustrated Lewis Pairs with Controlled Electronic and Steric Properties. *Organometallics* **2015,** *34*, 2000-2011.
62. A cross-peak signal is also observed between P3 and the aldehydic proton, however the signal of the latter overlaps with other protons in the 1H spectrum.
63. We reasoned that $SbCl_3$ (being ambiphilic due to the presence of a lone pair on Sb and easily cleaved Sb-Cl bonds) should be a suitable substrate for FLP-like activation by **3**.
64. Bader, R. *Atoms in molecules: a quantum theory*. Oxford University Press: 1994.
65. Lode, P.; Popelier, A. In *The Chemical Bond*; Frenking, G., Shaik, S., Ed.; 2014; Vol. 1, pp 271-308.
66. Shahbazian, S. Why Bond Critical Points Are Not "Bond" Critical Points. *Chem. Eur. J.* **2018,** *24*, 5401-5405.
67. Macchi, P.; Proserpio, D. M.; Sironi, A. Experimental Electron Density in a Transition Metal Dimer: Metal−Metal and Metal−Ligand Bonds. *J. Am. Chem. Soc.* **1998,** *120*, 13429-13435.
68. Macchi, P.; Sironi, A. Chemical bonding in transition metal carbonyl clusters: complementary analysis of theoretical and experimental electron densities. *Coord. Chem. Rev.* **2003,** *238-239*, 383-412.
69. Kocher, N.; Leusser, D.; Murso, A.; Stalke, D. Metal Coordination to the Formal P=N Bond of an Iminophosphorane and Charge-Density Evidence against Hypervalent Phosphorus(V). *Chem. Eur. J.* **2004,** *10*, 3622-3631.
70. Rahm, M.; Zeng, T.; Hoffmann, R. Electronegativity Seen as the Ground-State Average Valence Electron Binding Energy. *J. Am. Chem. Soc.* **2019,** *141*, 342-351.
71. We note in passing that the low DI for Ti-P1 is consistent with the unusually shielded (for a Ti(IV) phosphide) NMR signal of P1.
72. Connelly, S. J.; Kaminsky, W.; Heinekey, D. M. Structure and Solution Reactivity of (Triethylsilylium)triethylsilane Cations. *Organometallics* **2013,** *32*, 7478-7481.

73. Frisch, M. J.; Trucks, G. W.; Schlegel, H. B.; Scuseria, G. E.; Robb, M. A.; Cheeseman, J. R.; Scalmani, G.; Barone, V.; Petersson, G. A.; Nakatsuji, H.; Li, X.; Caricato, M.; Marenich, A. V.; J. Bloino, B. G. J.; R. Gomperts, B. M.; Hratchian, H. P.; Ortiz, J. V.; Izmaylov, A. F.; Sonnenberg, J. L.; Williams-Young, D.; Ding, F.; Lipparini, F.; Egidi, F.; Goings, J.; Peng, B.; Petrone, A.; Henderson, T.; Ranasinghe, D.; Zakrzewski, V. G.; Gao, J.; Rega, N.; Zheng, G.; Liang, W.; Hada, M.; Ehara, M.; Toyota, K.; Fukuda, R.; Hasegawa, J.; Ishida, M.; Nakajima, T.; Honda, Y.; Kitao, O.; Nakai, H.; Vreven, T.; Throssell, K.; J. A. Montgomery, J.; Peralta, J. E.; Ogliaro, F.; Bearpark, M. J.; Heyd, J. J.; Brothers, E. N.; Kudin, K. N.; Staroverov, V. N.; Keith, T. A.; Kobayashi, R.; Normand, J.; Raghavachari, K.; Rendell, A. P.; Burant, J. C.; Iyengar, S. S.; Tomasi, J.; Cossi, M.; Millam, J. M.; Klene, M.; Adamo, C.; Cammi, R.; Ochterski, J. W.; Martin, R. L.; Morokuma, K.; Farkas, O.; Foresman, J. B.; Fox, D. J. *Gaussian 16, Revision C.01*, 16, Revision C.01; Gaussian, Inc.: Wallingford CT, 2016.
74. Becke, A. D. Density-functional thermochemistry. III. The role of exact exchange. *J. Chem. Phys.* **1993,** *98*, 5648-5652.
75. Lee, C.; Yang, W.; Parr, R. G. Development of the Colle-Salvetti correlation-energy formula into a functional of the electron density. *Phys. Rev. B* **1988,** *37*, 785-789.
76. Vosko, S. H.; Wilk, L.; Nusair, M. Accurate spin-dependent electron liquid correlation energies for local spin density calculations: a critical analysis. *Can. J. Phys.* **1980,** *58*, 1200-1211.
77. Stephens, P. J.; Devlin, F. J.; Chabalowski, C. F.; Frisch, M. J. Ab Initio Calculation of Vibrational Absorption and Circular Dichroism Spectra Using Density Functional Force Fields. *J. Phys. Chem.* **1994,** *98*, 11623-11627.
78. Marenich, A. V.; Cramer, C. J.; Truhlar, D. G. Universal Solvation Model Based on Solute Electron Density and on a Continuum Model of the Solvent Defined by the Bulk Dielectric Constant and Atomic Surface Tensions. *J. Phys. Chem. B* **2009,** *113*, 6378-6396.
79. Grimme, S.; Ehrlich, S.; Goerigk, L. Effect of the damping function in dispersion corrected density functional theory. *J. Comput. Chem.* **2011,** *32*, 1456-1465.
80. Weigend, F.; Ahlrichs, R. Balanced basis sets of split valence, triple zeta valence and quadruple zeta valence quality for H to Rn: Design and assessment of accuracy. *Phys. Chem. Chem. Phys.* **2005,** *7*, 3297-3305.
81. P.Fleurat-Lessard, P. Dayal, Opt'n Path v1.50,freely available at: http://pfleurat.free.fr/ReactionPath.php, Last Visited: March 2022.
82. Bader, R. F. W. A quantum theory of molecular structure and its applications. *Chem. Rev.* **1991,** *91*, 893-928.
83. AIMAll (version 17.11.14B), T-A. Keith, TK Gristmill Software, Overland Park KS, USA, 2014
84. Kozlowski, D.; Pilmé, J. New insights in quantum chemical topology studies using numerical grid-based analyses. *J. Comput. Chem.* **2011,** *32*, 3207-3217.
85. https://www.lct.jussieu.fr/pagesperso/pilme/topchempage.html. (Last accessed 13 october 2021),
86. Humphrey, W.; Dalke, A.; Schulten, K. VMD: Visual molecular dynamics. *J. Mol. Graphics* **1996,** *14*, 33-38.
87. http://www.ks.uiuc.edu/Research/vmd/. . (Last accessed 13 october 2021),
88. C. Y. Legault, CYLview, 1.0b; Université de Sherbrooke, 2009 (http://www.cylview.org, Last Visited: March 2022.

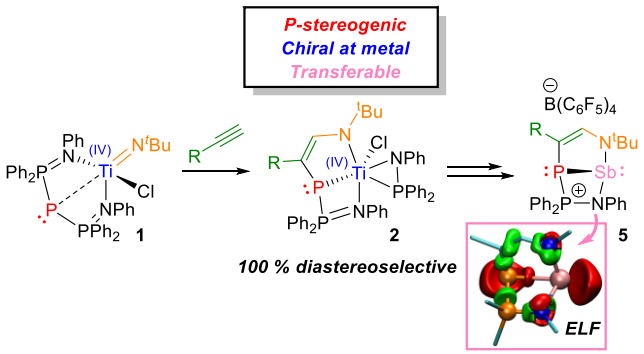

Synopsis : A Ti-imido complex supported by a bis(iminophosphoranyl)phosphide (BIPP) ligand undergoes a rearrangement in the presence of terminal alkynes, leading to the diastereoselective formation of Ti-bound pincer-type NPN' ligands. An NPN' ligand was transferred to Sb by transmetallation between a d^0 Ti-NPN' cation and $SbCl_3$. The bonding situation in the Ti- and Sb-NPN' cations was analyzed computationally, thus enabling the description of the NPN' ligands and their complexes in a chemically intuitive way.